

MMDVS-LF: A Multi-Modal Dynamic-Vision-Sensor Line Following Dataset

Felix Resch¹, Mónica Farsang¹, Radu Grosu¹

Abstract—Dynamic Vision Sensors (DVS), offer a unique advantage in control applications, due to their high temporal resolution, and asynchronous event-based data. Still, their adoption in machine learning algorithms remains limited. To address this gap, and promote the development of models that leverage the specific characteristics of DVS data, we introduce the Multi-Modal Dynamic-Vision-Sensor *Line Following* dataset (MMDVS-LF). This comprehensive dataset, is the first to integrate multiple sensor modalities, including DVS recordings, RGB video, odometry, and Inertial Measurement Unit (IMU) data, from a small-scale standardized vehicle. Additionally, the dataset includes eye-tracking and demographic data of drivers performing a *Line Following* task on a track. With its diverse range of data, MMDVS-LF opens new opportunities for developing deep learning algorithms, and conducting data science projects across various domains, supporting innovation in autonomous systems and control applications.

I. INTRODUCTION

Dynamic Vision Sensors (DVS) are an emerging visual-sensing technology, providing high-frequency asynchronous per-pixel intensity-change events, instead of full-image frames, at fixed intervals. The events provide a sparse representation of the observed scene, and modern sensors can achieve a per-pixel update rate of up to 10 kHz.

In this paper, we introduce a multi-modal DVS dataset, for a simple *Line Following* task, in a simplified environment. The aim is to encourage the development of novel, event-based neural-network theories, for event-based vision.

Currently, there are two approaches to applying machine learning (ML) methods to event-based data:

- Converting events in a certain time range to a frame representation, making it usable to a wide range of existing ML techniques
- Fully utilizing the sparse nature of DVS data using Spiking Neural Networks (SNNs)

While each frame representation requires a different trade-off between losing temporal information, or requiring a lot of storage and processing time, SNN simulations perform poorly on classic von Neumann architectures. As a consequence, they usually use specialized hardware[1].

State-of-the-art datasets for autonomous driving with DVS sensors, such as DDD17 [2] or its successor DDD20 [3], offer recordings of various driving scenarios. While this

F.R. and R.G. have received funding from the European Union’s Horizon Europe research and innovation program with Grant Agreement No. 10039070. M.F. has received funding from the European Union’s Horizon 2020 research and innovation programme under the Marie Skłodowska-Curie grant agreement No 101034277.

¹CPS, Technische Universität Wien (TU Wien), Austria

* E-mail of corresponding author: felix.resch@tuwien.ac.at

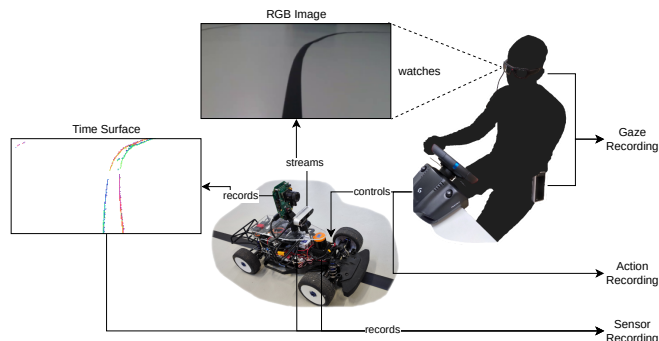


Fig. 1: Recording setup for dataset recording. The human driver views the RGB stream while wearing an eye-tracking headset and controlling the vehicle remotely.

enables networks to generalize well, developing new ML methods on datasets created for tasks as complex as street driving, is challenging. Even when only using a subset of the datasets, the environment is still very diverse and may contain observations not relevant to the task at hand.

The main challenge with datasets for complex tasks is that it is difficult to determine whether a potential new artificial-neural-network (ANN) architecture, fails to optimize due to a lack of hyperparameter tuning, or a faulty novel ML theory. We strongly believe that a dataset with reduced complexity could help to combat this issue. This paper introduces MMDVS-LF, a multi-modal DVS dataset for the *Line Following* task, recorded in a simplified environment.

In our simple *Line Following* task, the agent is equipped with a visual sensor, usually aimed at the floor, as the primary sensory input. The agent has to synthesize movement commands, to remain on a line marked on the floor, while continuously moving forward on that line. In addition to the visual input, the agent can receive additional information, such as inertial measurements or odometry data.

The data representation mentioned above, must balance temporal details, and representation size for ML approaches, that do not use the DVS event stream directly. Typical representations [4] for ANNs try to capture the input data in a fixed-size format, as most architectures require fixed-sized inputs. These representations provide formats similar to classical video frames for ANNs, to utilize established architectures by aggregating events in a specific time range. Some examples are event frames, which store the polarity of the last event per pixel; time surfaces, which store the last timestamps per pixel; and event tensors, which can represent multiple events per pixel, by further discretizing the time and aggregating events in those sub-steps.

TABLE I: Comparison of different Dynamic Vision Sensor (DVS) datasets for automotive applications. The first six datasets focus on computer-vision applications, while the others focus on control tasks. Checkmarks for the modalities indicate that data for this modality is available. Different annotation types: Manual = Manually annotated, Automatic = Algorithms were used, Implicit = Data is annotated directly from the recording.

Dataset	Task	Annotation	DVS	Inputs	IMU	RGB	Depth	Eye-Tracking	Amount
EventVOT [5]	Detection	Manual	1280x720			✓			249.92GB
FELT [6]	Detection	Manual	346x260			✓			664.78GB
1 MP Automotive [7]	Detection	Automatic	1280x720						15h/3.5TB
MVSEC [8]	Depth Estimation	Implicit	2x346x260		✓	2 x Gray	✓		186.62GB
DSEC [9]	Depth Estimation	Implicit	2x640x480		✓	2 x ✓	✓		453GB
Vivid++ [10] (Driving)	Visual SLAM	Implicit	640x480		✓	✓	✓		4:19h
Moeys et al. [11]	Following	Manual	36x36			✓			1:15h
DDD17 [2]	Driving	Implicit	346x260	✓		✓			12:00h
DDD20 [3]	Driving	Implicit	346x260	✓		✓			51:00h
MMDVS-LF (Ours)	Line Following	Manual	1280x720	✓	✓	✓	✓	✓	37:55m/11GB

MMDVS-LF consists of recordings from human drivers performing the *Line Following* task with F1Tenth [12] cars (standardized small-scale cars), in a simplified environment. We record: (1) The DVS event stream, (2) RGB-D frames, (3) IMU measurements, (4) Driving inputs, and (5) Eye-tracking data of the human drivers.

We recorded approximately 401 GB of raw data, from which we generated datasets with different resolutions and frequencies. All generated datasets remain below 15 GB in compressed size, and contain DVS time surface and event frame data, IMU measurements, and driving inputs. Due to its compact size, MMDVS-LF is easy to use and offers many application possibilities. This paper also demonstrates training established ANNs for a steering-prediction task, based on time-surface data from the dataset.

From the data collection and pre-processing point of view, we first give details of the recording procedure and processing pipeline for synchronizing and aligning the different modalities. Second, we describe our scaling methodology to scale down the DVS event data.

Based on MMDVS-LF, new ML architectures can be developed that fully utilize the sparse and asynchronous nature of DVS event streams. Moreover, the unique eye-tracking data also allows verifying ANNs by comparing their saliency information with human attention.

In summary, our contributions in this paper are as follows:

- MMDVS-LF, a dataset for a simple task with multiple resolutions, modalities, and frequencies.
- A method for collecting, synchronizing, and aligning multi-modal DVS datasets
- Potential use case for control application, showing how to use it with convolutional neural networks and those in combination with recurrent neural networks to take advantage of the temporal nature of the task.

We provide links to the dataset files and contact information for access to the raw data at <https://github.com/CPS-TUWien/mmdvs>.

II. RELATED WORK

First, we overview existing DVS datasets and compare those to our MMDVS-LF dataset. Then, we summarize the tasks defined from DVS data with deep learning solutions in existing literature.

A. DVS Datasets

Table I summarizes DVS datasets, which contain recordings for automotive applications for various tasks. The datasets in the first section of the table are designed for computer vision tasks, such as detection or visual reconstruction tasks, and contain no driving commands.

EventVOT [5], FELT [6], and Prophesee’s 1MP Automotive dataset [7] are designed for detection tasks, offering either raw event data or polarity-separated event frames and classified object boxes. Prophesee’s dataset exclusively contains traffic scenarios with various lighting conditions and traffic volume. It has been annotated by reconstructing frames from events and creating the bounding boxes using an established detection algorithm. EventVOT and FELT contain recordings of various situations, including automotive scenarios and have been annotated manually.

EventVOT and the 1MP Automotive dataset both use Prophesee’s EVK3 DVS sensor. This sensor records visual events at 1280 by 720 pixels with a maximum event rate per pixel of 10 kHz. FELT uses DVS346, a combined sensor that records DVS events and RGB pixel data on the same chip. This results in almost identical optical frames for event-based and RGB data.

MVSEC [8] and DSEC [9] are two datasets for 3D reconstruction and depth estimation using two DVS sensors and 3D LIDARs for ground truth depth data. They also include two frame-based cameras and inertial measurement units. While MVSEC only provides grayscale frames, DSEC provides RGB frames in the dataset. Both datasets use recorded ground-truth data as labels for ML approaches.

Vivid++ [10] is a dataset recorded for Visual SLAM with some recordings from automotive scenarios. It includes modalities similar to MVSEC and DSEC but with only one DVS and RGB sensor. Vivid++ obtains ground truth data from sensors in use during recording.

The second section of Table I lists datasets designed for learning control tasks. While there appears to be a larger number of computer vision datasets, the amount of datasets for control tasks is limited.

Moeys et al. [11] recorded a dataset for following a target and manually added high-level commands to reach the target. As high-level commands, they used a direction (left, center,

right) in which the target vehicle is located or "Not detected" to indicate that the target had not been detected yet. The available dataset contains low-resolution DVS event data and the manually annotated action.

DDD17 [2] and DDD20 [3] comprise multiple recordings of manual driving on public roads in various settings and situations. DDD17 contains approximately 12 hours of recordings, while DDD20 extends it with an additional 39 hours, resulting in 51 hours. Both include DVS and RGB data, driving commands, and vehicle telemetry data, such as speed, control position, and the state of various other vehicle components.

B. Benchmark Tasks

Many deep learning techniques have been applied to work with DVS data [13]. For optical flow estimation and object recognition tasks, methods such as the Synaptic Kernel Inverse Method (SKIM) [14], hierarchical Spiking Neural Networks [15], [16], and LSTM variants [7], [17], [18] have been utilized. Building on Convolutional Neural Networks (CNNs) [19], ResNet architectures [20] in [3], [21] and EV-FlowNet [22] were proposed to learn from event-based inputs. Additionally, [23] explored depth reconstruction using unsupervised learning with the Evenly-Cascaded Convolutional Network (ECN).

However, previous work related to control tasks using machine learning algorithms, the same way as available datasets for control, is limited. [11] employs CNNs to predict control commands for four classes of robot movements based on DVS data. This approach restricts the robot's controllability to discrete values. A setup more similar to our work is described in [24], where ResNet architectures are used for event frames to predict steering angles. In contrast, we aim to explore a broader range of network architectures by employing not only pure CNN-based solutions but also those incorporating recurrent networks.

III. DATASET

In this section, we describe the recording setup, the dataset annotation, the different formats of the MMDVS-LF dataset we provide, and statistical information.

A. Recording

We recorded the dataset on 1:10 scale racecars, based on the F1Tenth autonomous racing cars lecture by the University of Pennsylvania [12]. F1Tenth cars use chassis of commercially available 1:10 model racecars and are equipped with a computing platform, motor electronics, and sensors for environment perception. The sensors typically include a Hokuyo UST-10LX 270° 2D-Lidar [25] sensor and inertial measurement units. We use the Robot Operating System (ROS) [26] to run control software for the racecar.

We mounted an Intel realsense i435 in front of a Sony Prophesee IMX636 dynamic vision sensor (DVS) for the recording. The RGB video of the realsense camera is streamed to a screen in front of a human driver, who can control the car with a steering wheel and pedals. All other

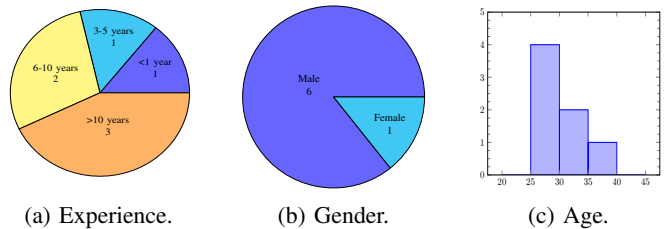


Fig. 2: Distribution of demographic data of the drivers in the MMDVS-LF dataset.

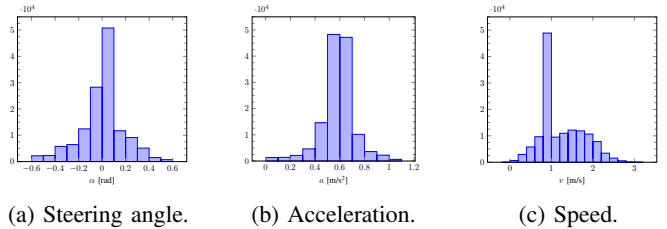


Fig. 3: Distribution of driving inputs, such as steering angle and acceleration command from the human drivers and speed measured by odometry.

data streams, including driving commands and depth data, are recorded on the car for later processing.

In addition to the driving data, we record eye-tracking (ET) data, of the human drivers using a VPS 19[27] ET system. We use ArUco [28] markers displayed on the screen showing the video to transform the ET video to the RGB stream. As we were streaming the RGB video to the control station, we recorded that stream separately to record the same stream the driver sees, including, for example, camera artifacts. The remaining data is recorded with tooling from the ROS ecosystem, which includes timestamps for each recorded datum. We used pulsed visual signals generated by LEDs observed by the DVS sensor and the RGB camera to synchronize the ROS recording and the RGB and ET streams.

For each recording, we gave the human driver a few minutes to get comfortable with the controls and the task before recording them driving in their training direction. After approximately four minutes, we interrupted the recording, turned the car around, and let the drivers drive in the opposite direction for another four minutes.

In addition to recording their driving, we asked participants to complete a consent form and a demographic questionnaire. This questionnaire collected their age, gender, country of origin and residence, and health details, including any chronic illnesses, visual impairments, or conditions affecting their vision. We also gathered information about their driving experience, including their length and frequency, professional or racing experience, prior experience with driving F1Tenth cars, comfort level with new technology, and whether they experience motion sickness while driving. Anonymized participants' data, including the mapping of the recordings to a driver, is available in the raw data.

Figure 2 displays the distribution of selected demographic data. For the *Line Following* task, we had seven participants, of whom six were born and obtained their driver's licenses in

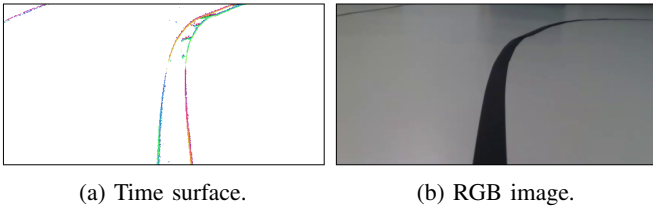


Fig. 4: Frame of the data used in the dataset. The time surface is on the left, and the RGB image is on the right. In the time surface, lighter areas indicate earlier events and darker areas later ones. The DVS and RGB camera optics have slightly different intrinsics, leading to different perspectives of the two images.

a country in Western Europe and one in North America. We had six male participants and one female participant, with an age distribution peaking at 25-30, including participants up to 35-40. One participant reported having no or less than one year of experience. Another participant reported 3-5 years of experience; two reported 6-10 years, and three more than ten years. Three participants reported that they have a visual impairment or use a visual aid for driving. Only one participant reported having a chronic illness, which impairs their driving skills, and one participant reported being a professional driver.

B. Annotation

We manually annotated the raw data to obtain sections of the recordings with desired behavior. All sections where, the line on the floor is visible in the bottom row of pixels, and where the driver managed to stay on or return to the line without losing it, were considered desired behavior. This extended acceptance leads to a broader range of recorded situations, which should also allow learning-based algorithms to learn recovering behaviors.

We also labeled possible sections that contain objects that have no direct influence on the *Line Following* task, but might interfere with computer vision applications. Examples are insects detected by the DVS only, and humans standing on or close to the line. The latter occurred in some recordings at the end to mark the end of the recording.

Due to differing lighting conditions in the recording area, the infrared lasers of the Intel realsense’s active depth estimation system were visible in some sections of the recordings. They introduced noise into the dataset recording, so we removed the areas with heavy noise from the generated DVS dataset. Some sections contained less noise, which we included in a separate dataset for more robust training.

We derive the action annotations from the human drivers’ driving commands and include observations from some sensors. Other sensors, such as LIDAR, were omitted from the dataset as they are irrelevant to the *Line Following* task.

C. Format

From the raw data recorded in Sec. III-A and the annotations, we generated frame-based datasets with frequencies

of 60 Hz, 100 Hz, and 120 Hz and image resolutions of 128x256 and 256x512. The dataset with 60 Hz includes RGB images, as we use a camera with 60 FPS for recording. We omitted the RGB images for datasets with higher frequencies to avoid using poor interpolation results. We treat events’ polarity separately for this dataset, generating two channels, one for each polarity.

To scale down the DVS data, we first crop the sensor area to a power of two and use virtual macro pixels. Each macro pixel stores an internal state, which counts increasing and decreasing events, with events of opposing polarity canceling each other out. Once that internal state exceeds the number of pixels in the macro pixel, the macro pixel generates an event with the respective polarity.

We generate time surfaces and event frames from the scaled-down event stream, as described in [7]. We also provide different sets of masks, which include filters and a mode we call *overwrite previous (owp)*. It removes events of opposite polarity if a more recent event occurs. This mode performed better during initial tests with classic-control approaches, allowing algorithms to interpret only the most recent data. We use neighborhood filtering to remove events from a frame if less than two other events occur in the adjacent pixels.

After generation, we store the dataset in compressed archives, storing each frame as `.npz` file. Storing each frame in separate files allows splitting and rearranging the datasets arbitrarily. Table II lists the arrays present in the archive and their values. We also include index files containing continuous sections of recordings to sample continuous sections from the dataset.

All `*mask` arrays represent event frames of the dataset. The `data` array might contain unfiltered arbitrary data, which must be combined with one `*mask` array. The `action` consists of the steering angle and either speed or acceleration commands. The `observation` array provides data from the IMU sensor, including acceleration in the (x,y,z) directions, angular velocity around these axes, and the orientation quaternion for (x,y,z,w) components. In addition to this, the `observation` also includes odometry information, such as pose estimation (x,y,z) , orientation quaternion for (x,y,z,w) , and velocity values along the (x,y,z) axes.

D. Statistics

We generate twelve datasets with time surfaces and event frames, actions, and observations, based on the different resolutions, frequencies, and the inclusion or exclusion of sections with a small amount of noise. While the representations differ in resolution and generation frequency, the underlying data is the same, and the resulting datasets have the same action distributions. The analysis in this section was performed on the 256x512@60Hz dataset, and light noise sections were included. Other datasets, especially the ones without the light noise sections, might differ slightly.

The generated datasets span 38 minutes, including noisy sections, or 27 minutes without those sections. Depending on the frequency, this leads to datasets of 96,161 to 272,838

TABLE II: Arrays present in a single frame file with their dimensions and a description of their contents. SIZE={512, 256} refers to the resolution size of the dataset.

Name	Dimension	Description
data	(SIZE/2, SIZE, 2)	Time until last event since start of frame per channel
mask	(SIZE/2, SIZE, 2)	Mask for valid data
action	(3)	Commanded action (steering angle, speed, acceleration)
observation	(20)	IMU and odometry sensor readings
filtered_mask	(SIZE/2, SIZE, 2)	Neighborhood filtered mask
owp_mask	(SIZE/2, SIZE, 2)	Overwrite (clear mask) of earlier events with opposing polarity
filtered_owp_mask	(SIZE/2, SIZE, 2)	Neighborhood filtered owp_mask

TABLE III: Number of frames and size of the compressed dataset for the different generated datasets. Values are indicated by the available data *with noise* / *without noise*. The 60 Hz version includes RGB data, while the 100 Hz and 120 Hz versions have DVS data only.

Noisy/No Noise	128x256	256x512
60 Hz	136,484 / 96,161 Frames 4.92 GB / 2.926 GB	10.98 GB / 7.462 GB
100 Hz	227,375 / 160,127 Frames 1.56 GB / 1.08 GB	4.98 GB / 3.45 GB
120 Hz	272,838 / 192,127 Frames 1.73 GB / 1.19 GB	5.42 GB / 3.75 GB

frames. Table III gives an overview of the size of the generated datasets and the compressed frames size sum.

Fig. 3 shows the distributions of the actions taken by the human drivers during the desirable driving sections. The steering angle’s distribution is symmetric with the mean at -0.006 rad, as seen in Fig. 3a. The standard deviation is 0.182 rad, which is expected, as large sections of the track are straight. As the cars were comparably heavy, no breaking was necessary, and only positive acceleration inputs (Fig. 3b) were recorded. The acceleration inputs have a mean of 0.586 m/s^2 and a standard deviation of 0.138 m/s^2 . Fig. 3c shows that a large portion of the driving occurred within the range of $0.6-2.0 \text{ m/s}$, with a peak at $0.8-1.0 \text{ m/s}$. This peak and the fact that most other observations have a higher speed allow training neural networks to only predict for steering angle, further simplifying the network architectures.

We recorded the MMDVS-LF’s data over about 8 hours, including instructions for the drivers, training, setup time, and technically required breaks, such as changing batteries. The annotation of the dataset took approximately four weeks, including regular updates of the annotation tools, as we discovered issues with our tooling or errors in annotation. Generating the dataset with our tooling takes approximately 36 hours on an Intel(R) Xeon(R) Gold 6130 machine with 20 CPU cores and 64 GB of RAM.

IV. BENCHMARK

The DVS data holds many promising directions for deep learning research. One can investigate which representation of the data fits better with existing machine learning algorithms or develop new ANN architectures that suit the unique characteristics of DVS data.

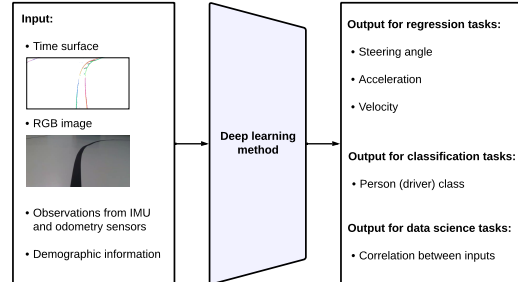


Fig. 5: Summary showing the different inputs for training deep learning models to predict various outputs using the MMDVS-LF dataset.

TABLE IV: Settings of the layers in the convolutional networks. Adapted from [29].

Layer Type	Settings
Input	Input shape: (128, 256, 2)
Conv2D	Filters: 24, Kernel size: 5, Stride: 2
Conv2D	Filters: 36, Kernel size: 5, Stride: 1
MaxPool2D	Pool size: 2, Stride: 2
Conv2D	Filters: 48, Kernel size: 3, Stride: 1
MaxPool2D	Pool size: 2, Stride: 2
Conv2D	Filters: 64, Kernel size: 3, Stride: 1
MaxPool2D	Pool size: 2, Stride: 2
Conv2D	Filters: 64, Kernel size: 3, Stride: 1
Flatten	-
Dense	Units: 64

A. Setups from the dataset

As summarized in Sec. II-B, most machine learning work on DVS data focused on optical flow and object recognition tasks. Here, we aim to highlight various other possibilities our MMDVS-LF dataset provides, such as control tasks (regression), driver identification (classification), and other data science tasks. Fig. 5 summarizes possible training setups using the dataset, including regression tasks predicting the steering angle with velocity or acceleration values based on various combinations of inputs. For classification tasks, one can consider the different drivers completing the *Line Following* task as class labels and use the available input data (excluding the demographic information) to make the prediction. Suppose someone aims to pursue a data science project. In that case, exploring the correlation between driving characteristics and demographic information or fault detection from the various sensor readings is possible.

TABLE V: Training, validation, and test losses of different architectures on the MMDVS-LF dataset. We found that all ANNs can converge to comparably the same training and validation loss values in the *Line Following* task, but only CNNs in combination with strong recurrent parts, such as LSTMs and LTCs, can generalize well on unseen data, which can be observed in the Test loss. Results are averaged over three runs.

Model	Training loss	Validation loss	Test loss
CNN	17.137 \pm 0.572	72.567 \pm 4.076	197.941 \pm 16.456
CNN + Simple RNN	16.090 \pm 0.499	75.223 \pm 0.437	197.605 \pm 12.809
CNN + MGU	15.790 \pm 0.740	69.077 \pm 2.009	196.521 \pm 20.303
CNN + GRU	15.187 \pm 0.745	74.633 \pm 1.095	180.543 \pm 12.349
CNN + LSTM	22.970 \pm 7.953	66.963 \pm 3.516	106.961 \pm 6.078
CNN + LTC	18.99 \pm 6.015	74.923 \pm 4.344	122.298 \pm 8.078

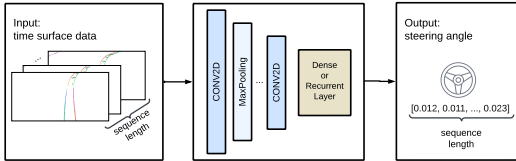


Fig. 6: For benchmarking, we use the following architecture: sequences of time surface data are created and fed into our neural networks of interest. These networks consist of several convolutional and max pooling layers, followed by a dense or recurrent network, which predicts the sequence of steering angles corresponding to the input.

B. Steering prediction from time surfaces

Here, we present a use case for the MMDVS-LF dataset of 128x256@100Hz, where the goal is to train neural network models to predict the steering angle based on the time surface data from the DVS sensor. As pointed out in Sec. III-D, most of the velocity values fall into a small range, allowing us to simplify the task by treating the speed as constant. The pipeline is illustrated in Fig. 6. We provide the code of a TensorFlow dataloader pipeline and training scripts.

We trained a convolutional-neural-network (CNN) front-end [19], with either a fully-connected dense layer, or a Recurrent Neural Network (RNN), respectively, as the back-end policy. As an RNN we used either a fully-connected simple RNN [30], a Minimal Gated United (MGU) [31], a Gated Recurrent Unit (GRU) [32], a Long-Short Term Memory (LSTM) [33], or a Liquid-Time Constant Network (LTC) [34], respectively. In these architectures, the CNN extracts visual information, while the RNN component leverages the sequential nature of the task. For configuring the CNN layers, we adapted the settings from the convolutional head used in [29], which was designed to explore the task of curvature prediction based on RGB images using a combination of CNNs and bio-inspired recurrent models. This adaptation is appropriate because, at a high level, our task is similar from an ML perspective.

We compute the mean squared error (MSE) between the predicted steering angle and the ground truth values over the sequences, scaling the errors by 10^4 for better readability. The data is split into training, validation and test sets with a ratio of 60%/20%/20%. We did hyperparameter tuning for the learning rate in the range of $\{0.0001, 0.001, 0.01\}$. Based on the best validation loss, we train all networks using a learning rate of 0.0001. During the training, we use the

AdamW optimizer [35] with a cosine weight decay of 10^{-6} . We run the training for 50 epochs and save the final models with the best validation loss.

The results of these experiments are shown in Table V. We found that all architectures were able to adapt to the task. Our results demonstrate that more sophisticated architectures incorporating recurrent networks generalized better on the MMDVS-LF dataset, leading to smaller loss values.

Here, we presented a simple setup from our MMDVS-LF dataset with a wide range of deep-learning approaches. This setup can be extended by using additional available information, such as stacking RGB channels to DVS as extra input channels to the CNN part, resulting in 5 channels (3 channels from RGB, two channels from DVS) in total, and mapping other sensor information of IMU and odometry to the dense or recurrent part. One can extend the output to making sequential predictions not only on the steering angle but also on the velocity or acceleration commands. In this case, one should adapt the loss function to $L = w_s \text{MSE}(y_s, \hat{y}_s) + w_v \text{MSE}(y_v, \hat{y}_v)$ to properly scale the mean squared errors of the used commands between the ground truth labels y_s, y_v and predictions \hat{y}_s, \hat{y}_v by the corresponding weights w_s, w_v , for the steering and velocity, respectively.

V. CONCLUSIONS

We introduced MMDVS-LF, a multimodal, compact, and easy-to-use dataset primarily intended for basic research, focusing on novel deep learning solutions leveraging sparse DVS data for control applications. The paper described the methods for recording experiments and constructing the dataset. We also showed several use cases of our dataset and demonstrated the power of recurrent neural networks predicting steering commands from time surface data.

In the future, we aim to explore DVS-specific control solutions and verify the attention maps of trained neural networks with the recorded eye-tracking data. The relatively inexpensive standardized platform of FITenth cars holds the potential to deploy end-to-end machine learning solutions on hardware, making it accessible to universities, research institutions, and the general public to test their solution developed and trained on the MMDVS-LF dataset.

ACKNOWLEDGMENT

We thank Mihaela-Larisa Clement for helping with the data collection and the participants in our recordings.

REFERENCES

- [1] M. Bouvier, A. Valentian, T. Mesquida, F. Rummens, M. Reyboz, E. Vianello, and E. Beigne, "Spiking neural networks hardware implementations and challenges: A survey," *J. Emerg. Technol. Comput. Syst.*, vol. 15, no. 2, apr 2019. [Online]. Available: <https://doi.org/10.1145/3304103>
- [2] J. Binas, D. Neil, S. Liu, and T. Delbrück, "DDD17: end-to-end DAVIS driving dataset," *CoRR*, vol. abs/1711.01458, 2017. [Online]. Available: <http://arxiv.org/abs/1711.01458>
- [3] Y. Hu, J. Binas, D. Neil, S.-C. Liu, and T. Delbruck, "Ddd20 end-to-end event camera driving dataset: Fusing frames and events with deep learning for improved steering prediction," in *2020 IEEE 23rd International Conference on Intelligent Transportation Systems (ITSC)*, 2020, pp. 1–6.
- [4] G. Gallego, T. Delbrück, G. Orchard, C. Bartolozzi, B. Taba, A. Censi, S. Leutenegger, A. J. Davison, J. Conradt, K. Daniilidis, and D. Scaramuzza, "Event-based vision: A survey," *IEEE Transactions on Pattern Analysis and Machine Intelligence*, vol. 44, no. 1, pp. 154–180, 2022.
- [5] X. Wang, S. Wang, C. Tang, L. Zhu, B. Jiang, Y. Tian, and J. Tang, "Event stream-based visual object tracking: A high-resolution benchmark dataset and a novel baseline," in *Proceedings of the IEEE/CVF Conference on Computer Vision and Pattern Recognition*, 2024, pp. 19 248–19 257.
- [6] X. Wang, J. Huang, S. Wang, C. Tang, B. Jiang, Y. Tian, J. Tang, and B. Luo, "Long-term frame-event visual tracking: Benchmark dataset and baseline," 2024.
- [7] E. Perot, P. de Tournemire, D. Nitti, J. Masci, and A. Sironi, "Learning to detect objects with a 1 megapixel event camera," in *Advances in Neural Information Processing Systems*, H. Larochelle, M. Ranzato, R. Hadsell, M. Balcan, and H. Lin, Eds., vol. 33. Curran Associates, Inc., 2020, pp. 16 639–16 652. [Online]. Available: https://proceedings.neurips.cc/paper_files/paper/2020/file/c213877427b46fa96cff6c39e837ccee-Paper.pdf
- [8] A. Z. Zhu, D. Thakur, T. Özarslan, B. Pfrommer, V. Kumar, and K. Daniilidis, "The multivehicle stereo event camera dataset: An event camera dataset for 3d perception," *IEEE Robotics and Automation Letters*, vol. 3, no. 3, pp. 2032–2039, 2018.
- [9] M. Gehrig, W. Aarents, D. Gehrig, and D. Scaramuzza, "Dsec: A stereo event camera dataset for driving scenarios," *IEEE Robotics and Automation Letters*, 2021.
- [10] A. J. Lee, Y. Cho, Y.-s. Shin, A. Kim, and H. Myung, "Vivid++: Vision for visibility dataset," *IEEE Robotics and Automation Letters*, vol. 7, no. 3, pp. 6282–6289, 2022.
- [11] D. P. Moeys, F. Corradi, E. Kerr, P. Vance, G. Das, D. Neil, D. Kerr, and T. Delbrück, "Steering a predator robot using a mixed frame/event-driven convolutional neural network," in *2016 Second international conference on event-based control, communication, and signal processing (EBCCSP)*. IEEE, 2016, pp. 1–8.
- [12] Esec6150: F1tenth autonomous racing cars. [Online]. Available: <https://f1tenth.org/course.html>
- [13] X. Zheng, Y. Liu, Y. Lu, T. Hua, T. Pan, W. Zhang, D. Tao, and L. Wang, "Deep learning for event-based vision: A comprehensive survey and benchmarks," *arXiv preprint arXiv:2302.08890*, 2023.
- [14] J. C. Tapsen, G. K. Cohen, S. Afshar, K. M. Stiefel, Y. Buskila, R. M. Wang, T. J. Hamilton, and A. van Schaik, "Synthesis of neural networks for spatio-temporal spike pattern recognition and processing," *Frontiers in neuroscience*, vol. 7, p. 153, 2013.
- [15] G. Orchard, C. Meyer, R. Etienne-Cummings, C. Posch, N. Thakor, and R. Benosman, "Hfirst: A temporal approach to object recognition," *IEEE transactions on pattern analysis and machine intelligence*, vol. 37, no. 10, pp. 2028–2040, 2015.
- [16] G. Orchard, A. Jayawant, G. K. Cohen, and N. Thakor, "Converting static image datasets to spiking neuromorphic datasets using saccades," *Frontiers in neuroscience*, vol. 9, p. 437, 2015.
- [17] D. Neil, M. Pfeiffer, and S.-C. Liu, "Phased lstm: Accelerating recurrent network training for long or event-based sequences," *Advances in neural information processing systems*, vol. 29, 2016.
- [18] M. Cannici, M. Ciccone, A. Romanoni, and M. Matteucci, "A differentiable recurrent surface for asynchronous event-based data," in *Computer Vision—ECCV 2020: 16th European Conference, Glasgow, UK, August 23–28, 2020, Proceedings, Part XX 16*. Springer, 2020, pp. 136–152.
- [19] Y. LeCun, B. Boser, J. Denker, D. Henderson, R. Howard, W. Hubbard, and L. Jackel, "Handwritten digit recognition with

- a back-propagation network,” in *Advances in Neural Information Processing Systems*, D. Touretzky, Ed., vol. 2. Morgan-Kaufmann, 1989. [Online]. Available: https://proceedings.neurips.cc/paper_files/paper/1989/file/53c3bce66e43be4f209556518c2fcb54-Paper.pdf
- [20] K. He, X. Zhang, S. Ren, and J. Sun, “Deep residual learning for image recognition,” in *Proceedings of the IEEE conference on computer vision and pattern recognition*, 2016, pp. 770–778.
- [21] D. Gehrig, A. Loquercio, K. G. Derpanis, and D. Scaramuzza, “End-to-end learning of representations for asynchronous event-based data,” in *Proceedings of the IEEE/CVF International Conference on Computer Vision*, 2019, pp. 5633–5643.
- [22] A. Z. Zhu, L. Yuan, K. Chaney, and K. Daniilidis, “Ev-flownet: Self-supervised optical flow estimation for event-based cameras,” *arXiv preprint arXiv:1802.06898*, 2018.
- [23] C. Ye, A. Mitrokhin, C. Fermüller, J. A. Yorke, and Y. Aloimonos, “Unsupervised learning of dense optical flow, depth and egomotion with event-based sensors,” in *2020 IEEE/RSJ International Conference on Intelligent Robots and Systems (IROS)*, 2020, pp. 5831–5838.
- [24] A. I. Maqueda, A. Loquercio, G. Gallego, N. García, and D. Scaramuzza, “Event-based vision meets deep learning on steering prediction for self-driving cars,” in *Proceedings of the IEEE conference on computer vision and pattern recognition*, 2018, pp. 5419–5427.
- [25] UST-10lx :: Sentek hokuyo. [Online]. Available: <https://hokuyo-usa.com/products/lidar-obstacle-detection/ust-10lx>
- [26] ROS: Home. [Online]. Available: <https://www.ros.org/>
- [27] Vps 19: Ready for immediate remote support and streaming. [Online]. Available: <https://viewpointssystem.com/en/products-new/vps-19/>
- [28] S. Garrido-Jurado, R. Muñoz-Salinas, F. Madrid-Cuevas, and R. Medina-Carnicer, “Generation of fiducial marker dictionaries using mixed integer linear programming,” *Pattern Recognition*, vol. 51, pp. 481–491, 2016. [Online]. Available: <https://www.sciencedirect.com/science/article/pii/S0031320315003544>
- [29] M. Farsang, M. Lechner, D. Lung, R. Hasani, D. Rus, and R. Grosu, “Learning with chemical versus electrical synapses does it make a difference?” in *2024 IEEE International Conference on Robotics and Automation (ICRA)*, 2024, pp. 15 106–15 112.
- [30] F. Chollet *et al.*, “Keras,” <https://keras.io>, 2015.
- [31] G.-B. Zhou, J. Wu, C.-L. Zhang, and Z.-H. Zhou, “Minimal gated unit for recurrent neural networks,” *International Journal of Automation and Computing*, vol. 13, no. 3, pp. 226–234, 2016.
- [32] K. Cho, B. van Merriënboer, Çağlar Gülçehre, D. Bahdanau, F. Bougares, H. Schwenk, and Y. Bengio, “Learning phrase representations using rnn encoder–decoder for statistical machine translation,” in *Conference on Empirical Methods in Natural Language Processing*, 2014.
- [33] S. Hochreiter and J. Schmidhuber, “Long short-term memory,” *Neural Comput.*, vol. 9, no. 8, p. 1735–1780, nov 1997. [Online]. Available: <https://doi.org/10.1162/neco.1997.9.8.1735>
- [34] R. M. Hasani, M. Lechner, A. Amini, D. Rus, and R. Grosu, “Liquid time-constant networks,” in *AAAI Conference on Artificial Intelligence*, 2020.
- [35] I. Loshchilov and F. Hutter, “Fixing weight decay regularization in adam,” *ArXiv*, vol. abs/1711.05101, 2017.